This is a pre-print of the following chapter:
Kriebel CN, Becker-Baldus J, Glaubitz C. Solid-state NMR spectroscopy on icrobial rhodopsins. **Methods Mol Biol** 2022;2501:181-206.
reproduced with permission of Springer Nature 2022.
The final authenticated version is available online at:
https://dx.doi.org/10.1007/978-1-0716-2329-9_9

Thematic Issue / Methods in Molecular Biology: Rhodopsins

Solid-state NMR Spectroscopy on Microbial Rhodopsins

Clara Nassrin Kriebel, Johanna Becker-Baldus and Clemens Glaubitz

Institute of Biophysical Chemistry
and
Centre for Biomolecular Magnetic Resonance
Goethe University Frankfurt
Max von Laue Str. 9
60438 Frankfurt am Main
Germany
glaubitz@em.uni-frankfurt.de
www.glaubitz-lab.de

Abstract

Microbial rhodopsins represent the most abundant phototrophic systems known today. A similar molecular architecture with 7 transmembrane helices and a retinal cofactor linked to a lysine in helix 7 enables a wide range of functions including ion pumping, light-controlled ion channel gating or sensing. Deciphering their molecular mechanisms requires therefore a combined consideration of structural, functional and spectroscopic data in order to identify key factors determining their function. Important insight can be gained by solid-state NMR spectroscopy by which the large homo-oligomeric rhodopsin complexes can be studied directly within lipid bilayers. This chapter describes the methodological background and the necessary sample preparation requirements for the study of photointermediates, for analysis of protonation states, H-bonding and chromophore conformations, for 3D structure determination and for probing oligomer interfaces of microbial rhodopsins. The use of data extracted from these NMR experiments is discussed in the context of complementary biophysical methods.

Key Words

microbial rhodopsin, retinal, structure, oligomer, photointermediate, solid-state NMR, MAS, dynamic nuclear polarization, PRE, *in situ* illumination

1. Introduction

General Background

The discovery of proteorhodopsin as the first bacterial rhodopsin about 20 years ago has triggered a paradigm shift: Until then the extensively studied archaeal bacteriorhodopsin had served as an important 'innovation engine' for the development of many biophysical methods for membrane protein research (e.g. cryo-EM, solid-state NMR, X-ray crystallography etc., see e.g. [1]). However, it was also considered an oddity of less evolutionary importance because of the rare occurrence of its extremophile host *H. salinarium*. This view has changed dramatically with rhodopsins found in all phyla of life covering a wide spectrum of functions. They represent actually the most abundant phototrophic systems known to date [2,3]. At the heart of research efforts in this field lies the question how a rather similar structural fold with seven transmembrane helices and an all-*trans* retinal chromophore bound to a conserved lysine is able to yield such a diverse array of functions ranging from ion pumps via channels to sensors. Examples are proteorhodopsin (PR) working as light-driven proton pump [4], the light-driven sodium pump KR2 [5], channelrhodopsin-2 (ChR2) functioning as a light-gated ion channel [6] and Anabaena sensory rhodopsin (ASR), a photosensor for chromatic adaptation [7].

To address this question, a deep mechanistic insight on the molecular level needs to be derived coupling functional characterization with optical properties, photocycle kinetics and 3D structures.

Solid-state NMR offers here unique opportunities since on the one hand, full 3D structure can be determined [8]. On the other hand, also very fine details usually beyond the resolution of X-ray structures such as C-C bond length distortions [9], out-of-plane twists within the retinal chromophore [10], retinal interaction with residues within the binding pocket [11,12] or the characterization of hydrogen bonds at the Schiff base nitrogen [13] or other residues [14] can be obtained in a site-resolved way. These details are needed to understand for example counter ion interactions or colour tuning. Recognizing subtle differences between rhodopsins will have a significant impact for the understanding of their functional mechanism. It became also increasingly clear that these proteins form homo-oligomers, with mainly trimers in case of archaea and predominantly pentamers in case of eubacteria [15]. These large complexes including their lipid bilayer environment can be studied directly using solid-state NMR spectroscopy. In this chapter we describe briefly the general technical background as well as sample preparation requirements and provide details on how photointermediates can be studied, how 3D structures can be determined and how oligomerisation interfaces can be probed.

Solid-state NMR spectroscopy

Most NMR interactions are anisotropic, i.e. orientation-dependent with respect to the magnetic field, which yields broad and complex line shapes. These interactions are averaged to their isotropic value if the molecules are soluble and tumble fast enough, which is however not the case for large, homo-oligomeric, membrane-embedded proteins such as rhodopsins. A solution is offered by magic angle sample spinning (MAS) by which these interactions are averaged through fast macroscopic sample rotation (Fig. 1a). A typical 2D NCA correlation spectrum of the uniformly ^{13}C, ^{15}N-labelled sodium pump KR2 within lipid bilayers is shown in Fig. 1b (left). Spectra are usually recorded via ^{13}C detection and resonance assignments become possible through 3D correlation experiments [16-18], which is the requirement for further structure and dynamic analysis.

In contrast to solution state NMR, direct detection of protons is challenging since they form a strong, homogeneous dipole-dipole coupling network leading to severe line broadenings under conditions of non-isotropic or reduced molecular mobility. Shrinking the outer diameter of the MAS rotors down to 0.7 mm (Fig. 1a, right) enables sample rotation rates of up to 110 kHz leading to improved ^{1}H resolution as demonstrated here for a ^{1}H-detected NH-MAS NMR spectrum of uniformly ^{15}N-labelled KR2 (Fig. 1b, middle). Resonance assignment using fully protonated lipid-embedded proteorhodopsin in such a small rotor has already been achieved [19]. For proton detection at slower MAS rates, additional sample deuteration would be needed [20]. Despite of the significant reduction in sample volume, the detection sensitivity of this approach is good due to the high intrinsic sensitivity of protons and because of the high efficiency of MAS probe heads with small radio frequency coils.

A fundamental increase in detection sensitivity is offered by dynamic nuclear polarization (DNP) [21,22]. A non-Boltzmann nuclear magnetization is created by utilizing stable biradicals such as AMUPol [23] as polarizers and by strong microwave irradiation during the MAS NMR experiment (Fig. 1a, left, middle). The microwave frequency has to match the electron Larmor frequency at the used magnetic field (e.g. 263 GHz / 400 MHz at 9 T). As a result, significant signal enhancement can be achieved. Values of 50-80 have been typically reported for rhodopsins enabling a 2500-6400-times faster data acquisition [13,24]. An example for the signal enhancement of the ^{13}C resonances of retinal within KR2 is shown in Fig. 1b (right) [16]. DNP works best under cryogenic conditions on frozen samples, which is a perfect match with the requirements for trapping of photocycle intermediates. To create such intermediates, *in situ* photo irradiation within the NMR spectrometer is used (Fig. 1a, left) as described below.

2. General sample preparation requirements

For MAS-NMR, the sample of interest has to be enriched with ^{13}C and ^{15}N. Such isotope enrichment is possible for the retinal and the protein itself. For retinal, numerous labelling schemes involving single, double, multiple and even uniform ^{13}C labelling have been used all based on *in vitro* synthesis [25-27,9,28,11]. The preparation of U-^{13}C retinal has even been shown biosynthetically using a prototrophic *E. coli* strain which was transformed with plasmids expressing retinal-producing enzymes [29]. The labelled retinal needs to be incorporated into the opsin of interest. This can either be achieved by adding it directly to the growth medium, which is however material intensive, or by adding it to the opsin either in the non-purified, crude [16,30] membrane fraction or during solubilisation [24]. In cases in which the opsin cannot be stably expressed, a bleaching step can be used at that stage for exchanging unlabelled with labelled retinal [31].

Many of the novel microbial rhodopsins discovered since 2000 can be conveniently expressed in *E. coli*, which offers a multitude of isotope labelling options since *E. coli* can be grown on a minimal medium in which ^{13}C and ^{15}N enriched carbon and nitrogen sources (glucose, glycerol, ammonium) can be used. The type of labelling scheme depends on the experimental aims and the choice of the MAS-NMR approach. Uniform ^{13}C and ^{15}N labelled samples are usually used for the structure and dynamic characterization of microbial rhodopsins in their ground states. These experiments are carried out on non-frozen samples at high magnetic fields resulting usually in high spectral resolution so that a large number of site-resolved data can be obtained simultaneously. In addition, ultra-fast MAS-NMR for direct ^{1}H detection often requires deuterated samples in which exchangeable sites have been re-protonated. DNP-enhanced MAS-NMR is performed on frozen samples and often on lower magnetic fields, which results in less well-resolved spectra. Therefore, in order to reduce spectral complexity, often amino-acid selective labelling is applied (for a recent review on such labelling options in *E. coli* see [32]). Even a perspective for segmental labelling has been demonstrated for proteorhodopsin, which would further reduce spectral complexity [33]. For eukaryotic microbial rhodopsins such as ChR2 and others, ^{13}C as well as ^{15}N isotope labelling options in *P. pastoris* have been successfully demonstrated, which significantly extends the applicability of the approaches shown here [34,35,30]. In contrast to bacteriorhodopsin, which can be readily used for MAS-NMR in its native purple membrane, all other microbial rhodopsins are usually purified from the membrane and then reconstituted into lipid bilayers to form proteoliposomes. It is however noteworthy, that the possibility to record MAS-NMR spectra of ASR directly within the inner *E. coli* membrane without further purification has been demonstrated [36]. For the NMR measurement, the proteoliposomes/membrane fractions are collected into MAS rotors by a centrifugation step.

Depending on the experimental strategies, further sample modifications might be helpful. For example, the data acquisition time can be shortened by 'doping' the samples with paramagnetic compounds such as Gd-DOTA (Fig. 1a), which does not interact with the rhodopsins or the bilayer but reduces the spin-lattice relaxation time of protons efficiently within the whole sample as demonstrated for green PR [37]. For DNP, as mentioned above, stable biradicals have to be added to the sample as polarization source. In case of BR, purple membrane patches are dispersed in 'DNP juice' (60% D_8-Glycerol, 30% D_2O and 10% H_2O (v/v/v) with 10 mM AMUPol) [13], while proteoliposome pellets are best incubated with a top layer of 30% D_8-Glycerol, 60% D_2O and 10% H_2O (v/v/v) with 20 mM AMUPol, which is then removed before the experiment (see [38]).

Labelling of cysteines by stable radicals offers additional options to obtain complementary long-range restraints via paramagnetic relaxation enhancement (PRE) [37,39] and for site-selective DNP or spectral editing [40].

3. Chromophore and photocycle intermediate states

Light-induced cryo-trapping and NMR spectroscopy

Solid-state NMR has been extensively used for the analysis of photointermediate states of microbial rhodopsins (for an overview see [41,38]). These studies focus primarily on the active site, i.e. the retinal Schiff base (RSB) complex and its counter ion interactions and rely on trapping of photointermediates after photoirradiation under MAS-NMR conditions.

A typical microbial rhodopsin photocycle is shown in Fig. 2a for proteorhodopsin [42]. In the ground state, the chromophore is in the all-*trans*, 15-*anti* conformation. An exception is found in dark-adapted BR with an equilibrium between all-*trans*,15-*anti* and 13-*cis*,15-*syn* retinal [43]. Upon light-absorption, the retinal switches from an all-*trans*,15-*anti* to 13-*cis*,15-*anti* conformation, which leads to the K state. This process is fast and initial evidence exists that also the protein environment in some rhodopsins starts to respond on the same timescale [44]. The absorption maximum is red shifted with respect to the ground state. Next, the protein prepares for the Schiff base deprotonation step which is, in some microbial rhodopsins, associated with the formation of a kinetically distinct L-intermediate. Subsequently, the strongly blue shifted M-intermediate with the deprotonated Schiff base forms. Its reprotonation usually causes the formation of the N-state and reconversion of the chromophore from 13-*cis* to the all-*trans* creates the red-shifted O-state followed by relaxation back to the ground state.

In order to derive mechanistic models for the multiple functions fulfilled by microbial rhodopsins, it is essential to precisely understand structure, dynamics, and interactions within and between RSB and opsin in all intermediates. Solid-state NMR can provide unique information on the chromophore

conformation, chromophore-opsin interactions and rearrangements within the opsin provided that these intermediates can be trapped.

In some cases, certain intermediates exhibit a much longer half-life than the other states. Such a situation offers the opportunity for *stationary trapping* of these states by continuous light irradiation since the production rate exceeds the relaxation rate. Examples are the extremely long-lived sensory rhodopsin II M-state (for a recent review on solid-state NMR on the SR II photocycle see [41]) and the desensitized state in ChR2 [30]. Another example is the elongation of the life time of certain photointermediate states by mutations as shown for the proton donor mutant E108Q in PR which enables enrichment of the M-state [24]. In the latter two examples the stationary generated states were then trapped using a freeze quench approach. In all other cases, specific schemes for light-induced cryo-trapping have to be applied and have been especially well worked out for bacteriorhodopsin [13]. Exact protocols depend very much on the specific protein characteristics (optical absorption properties, intermediate half-life, intermediate populations, thermal equilibria between intermediates), but the general approach can be illustrated based on the schematic energy landscape for the different intermediates in Fig. 2b: The K-state can be generated by illuminating the sample at low temperatures (around 100 K), which prevents its decay. Generally, a mixture between ground and K-state is obtained because absorption maxima overlap and K is converted back. By a subsequent rise in temperature, further intermediates can become accessible through the additional thermal energy ('thermal relaxation'). The intermediates trapped in this way depend very much on the protein-specific energy landscape and the particulars of the applied thermal relaxation protocol. Alternatively, sample illumination with the intermediate-specific wavelength at a suitable temperature can be used ('thermal trapping'). For example, in case of light-adapted BR, the K-state is trapped by green light at 90K, the L-state by red light at 150 K, the M-state by green light at 210 K and the N-state by red light at 240 K [13]. The duration of illumination also depends on the sample (optical density) and ranges between minutes to hours. This approach can result in an almost complete elimination of ground state populations in the sample. However, phenomena such as blue-light quenching in PR create an additional pathway back to the ground state [45] or photocycle branching can result in side product usually not observed using the thermal relaxation approach, which has to be considered when designing trapping experiments for a particular rhodopsin.

These trapping schemes can be implemented into the MAS-NMR experiment as shown in Fig. 2c. First of all, sufficient light-penetration into the proteoliposomes within the MAS rotors has to be achieved. Usually, transparent MAS rotors made of sapphire are used (Fig. 1a, right). For *in situ* illumination, the MAS NMR probe head is modified with a suitable multimode fibre to couple light during the MAS-NMR experiment directly into the sample. Lasers as well as high power LEDs are suitable light sources.

Instead of optically dense proteoliposome pellets, thin proteoliposome films spread on the inner surface of the MAS rotors turned out to enable a good trapping efficiency [30].

Highest sensitivity is a crucial factor especially for the detection and analysis of less-populated intermediates. Dynamic nuclear polarization in combination with *in situ* sample illumination offers here unprecedent possibilities. These experiments are fairly complex as light, microwave and multiple rf-frequency channels have to be coupled into the sample, but the significant gain in sensitivity enables experiments, which could not be carried out by conventional MAS-NMR.

DNP experiments are carried out usually in the temperature range between 90 and 110 K, which is also a perfect match for cryo-trapping of photointermediates. The temperature variation/illumination schemes described above always include a detection step at the end which is carried out in this temperature range (Fig. 2c). *In situ* illumination is certainly the preferred and most elegant way for creating photointermediates. There are however cases in which certain intermediates can only be prepared under continuous illumination of non-frozen samples followed by trapping through freeze-quenching. This step cannot easily be performed *in situ* as the cooling rate within the magnet is not fast enough. Therefore, freeze-quenching outside by dropping the MAS rotor into liquid nitrogen (Fig, 2c) followed by fast transfer into the pre-cooled MAS probe head has to be performed. An improved method for rapid freeze-quenching has recently been demonstrated for DNP-enhanced solid-state NMR applications [46], which might also help to extend the range of accessible photointermediates and to improve trapping efficiency.

The retinal-Schiff base complex during the photocycle

The first step in understanding the optical properties of microbial rhodopsins and the link between photocycle and their ion pumping activity is to elucidate the chromophore structure since it transfers the absorbed photon energy into the protein leading to protonation/de-protonation steps which couples back to the chromophore during the photocycle.

It is therefore helpful to summarize briefly key NMR parameters which define isomerization and protonation state of the RSB as shown in Fig. 3a. The isomerisation from all-*trans* (i) to 13-*cis* (ii) releases the steric interaction between C20 and C15 and creates a new steric contact between C12 and C15 [47,48]. Therefore, chemical shift changes are observed as C20 becomes more deshielded and C12 more shielded. The C12-C15 or C20-C15 distances can also be used to differentiate both isomers by determining their dipole-dipole couplings. The steric interaction between C14 and Lys-Cε in 15-*syn* retinal (iii) leads to an increased shielding of both atoms [49] and shorter distance between them compared to 15-*anti* [50]. In the ground state, the all-*trans* retinal Schiff base is protonated and positively charged (i). The charge is partially delocalized to the C13 atom (v). Deprotonation removes this charge (iv) and results in a very large deshielding of the nitrogen by more than 100 ppm [51] and

a significant shielding of C13. In microbial rhodopsins the chromophore is found in its 6-s-*trans* form whereas in visual rhodopsins a skewed 6-s-*cis* conformation is found (vi). A planar 6-s-*cis* conformation is unfavourable because of a steric clash between C18 and C8. The skewing of the ring weakens the conjugation of the C5 double bond with the π-system resulting in a shielding of C5 [47].

Besides of these well-established chemical shift markers, numerous additional parameters can be extracted, which can define the RSB conformation to high precision. The Schiff base ^{15}N chemical shift depends on the C15-N torsion but also to a large extent on the strength of the H-bond in which it might be involved, which is usually to the counter ion and which again correlates with the optical absorption maximum of the particular rhodopsin. The H-bond character can be further defined by determining the N-H bond length through dipolar distance measurements and by determining the proton chemical shift (see example below). Bond lengths distortion along the polyene chain can be determined by measuring C-C dipole couplings of directly bonded carbons [52,9], while drilling along the chain is accessible via H-C-C-H torsion angle measurements [24,53].

The effects of changes in the chromophore conformation are shown in Fig. 3b for green PR in the K- and M-state. Illumination and trapping at 110 K leads to an additional shielding of C12 and a de-shielding of C20 [11,24] indicative of the transition from 13-*anti* to 13-*cis*. Upon M-state trapping, a large additional shielding of C13 is observed and the signal splits into two populations arising from two trapped M-states. The Schiff base nitrogen resonance shifts from 181 ppm in its protonated form to 312 and 316 ppm upon deprotonation in both M-states [24].

A combined thermal trapping/relaxation approach is illustrated in Fig. 3c for the light-gated ion channel ChR2 [30]. In the dark state, the retinal is solely in the all-*trans*, 15-*anti* form. Upon illumination at 110 K, the K-like state P_1^{500} is formed. Cryo-UV/VIS spectroscopy can be used as an additional control for correct trapping (Fig. 3c). Further thermal relaxation steps show its decay and the gradual rise of the P_4^{480} state, which is the desensitized state after channel closure. C14 is additionally shielded indicative of the formation of a 15-*syn* conformation. Interestingly, illumination of P_4^{480} de-populates the ground state $ChR2^{470}$ and leads to another photoproduct (P_x), which has not been observed by optical spectroscopy.

Initially, retinal extraction experiments followed by HPLC analysis were the standard way to determine the chromophore confirmation in retinal proteins. However, the invasive nature of this method led to unreliable results. In addition, the information on the 15-bond is lost and it is rarely possible to analyse photointermediate states. Vibrational spectroscopy and especially Resonance Raman spectroscopy is much more powerful and non-invasive. However, band assignment is not trivial. The vibrational bands are superpositions of many modes and it is difficult to obtain localized information. In contrast, assignment of NMR chemical shifts is often straightforward, especially with selectively labelled retinal, and provides very localized information. The observed chemical shift changes due to bond-

isomerization are large and easy to interpret. Solid-state NMR spectroscopy should therefore be the method of choice to analyse the chromophore conformation.

Probing specific residues during the photocycle

The different trapping methods cannot only be used to follow the RSB throughout the photocycle but can be expanded towards monitoring the protein response in a site-resolved manner (by introducing suitable isotope labelling schemes) as illustrated for two specific cases below.

A seminal example for the power and importance of the methods described above is a recent DNP study on the unknown primary proton transfer step in BR [13]. The aim was to discriminate between proton transfer pathways put forward by QM/MM simulations, which either involve a direct transfer from SB to Asp85, a diversion via Asp212, Water 402 to Asp85 or a relay from SB via Thr89 to Asp85 [54]. The issue could be solved by determining the Schiff base ^{15}N and ^{1}H chemical shifts and the ^{15}N-^{1}H distances throughout the photocycle. Suitable trapping conditions have been established for almost all photointermediates in bacteriorhodopsin. In BR, the ^{15}N chemical shifts of the intermediates are well known and can be used to identify the trapped states in the spectra. Proton chemical shifts were determined via 2D ^{15}N-^{1}H HETCOR and distances measured by DIPSHIFT experiments. Surprisingly, the de-protonated nitrogen in the M_0 state shows a through-space correlation to an alcohol proton within H-bond distance (1.45 Å) assigned to Thr89 as proton donor. ^{13}C-^{13}C through-space correlation experiments also establish a closer interaction between Thr89 and the primary proton acceptor Asp85 the L- and M_0-state, i.e. prior and after the proton transfer step. In addition, the distance between the SB nitrogen and Asp85-Cγ is shortened in M_0 while the distance to Asp212-Cγ does not change during the photocycle, which reflects helices C and G moving closer to each other before the proton transfer step and relaxing afterwards. These data clearly show that the proton is indeed relayed to Asp85 via Thr89. It is important to point out that such fine details are difficult to obtain by X-ray crystallography.

In another case, selective DNP based on methyl-labelling was used to monitor changes in the retinal interaction with green PR [11]: The signal of the ^{13}C nuclei in the retinal C20 methyl group could be selectively increased by transferring the DNP-enhanced proton magnetization from the methyl protons (though hetNOE). The created carbon magnetization was then transferred (by spin diffusion) to ^{13}C-labelled residues within the retinal binding pocket in order to probe packing and conformational changes upon light-induced K-state formation. It could be shown that the C20 packing against the opsin is tighter in the K-state compared to the ground state providing experimental evidence for the role of C20 in the first steps of the photocycle. In contrast, the bulky residues in the binding pocket did not react upon the initial retinal isomerization.

Light-induced cryo-trapping of selectively labelled samples also enabled the discovery of photocycle dependent conformational changes at PR protomer interfaces as highlighted below.

4. 3D Structure determination of microbial rhodopsins

Solid-state NMR not only enables hypothesis-driven experiments, as outlines above on photointermediates, but also offers the possibility of complete 3D structure determinations of membrane proteins. Although rather challenging, this approach is attractive despite tremendous progress in X-ray crystallography and cryo-EM, because it is accessible to full oligomeric rhodopsin complexes within lipid bilayers at native-like pH and salt concentrations and under non-freezing conditions. A milestone example has been the structure determination of Anabaena sensory rhodopsin (ASR), [8]. ASR mediates signal transfer via a small soluble cytoplasmic protein between membrane and DNA in order to regulate the expression of proteins involved in photosynthesis and circadian rhythm [7]. In the following for the case of ASR, all necessary steps needed for the 3D structure determination of membrane proteins are outlined as summarised in Fig. 4.

Resonance assignment

The first prerequisite for a successful NMR structure calculation is a full ^{13}C, ^{15}N NMR resonance assignment. For resolving all ^{13}C and ^{15}N resonances, high magnetic fields (>700 MHz) and a set of multidimensional (2D-4D) correlation experiments are required. Obtaining highly resolved spectra depends on sample homogeneity and intrinsic protein dynamics. Typically, a set of 3D spectra such as NCACX, NCOCX and CONCA are recorded by which a sequential assignment along the backbone and into the side chains can be achieved. In case of ASR, three samples were prepared. Uniform ^{13}C and ^{15}N labelling allows assigning already a large set of resonances. Remaining spectral overlap was dealt with by using 1,3- and 2-^{13}C glycerol as a carbon source, which results in a reduced ^{13}C-labelling pattern [55]. Often, additional labelling schemes are used to reduce spectral overlap, which include ^{13}C, ^{15}N labelling of only few particular amino acid types (forward labelling) or suppress labelling of certain amino acid types (reverse labelling) or by using specifically labelled amino acids (selective labelling).

Distance restraints

The obtained chemical shifts already provide dihedral angle restraints, which define secondary structure regions within the protein [56,57]. For a 3D structure, a large number of additional internuclear distance restraints is needed. Furthermore, the arrangement of the protomers within the oligomeric complex and the oligomerization interfaces have to be resolved. In addition, in case of microbial rhodopsins, special attention has to be drawn to protein-chromophore contacts which significantly stabilize these seven-helical transmembrane proteins. Therefore, as many short-, medium- and long-range restraints as possible need to be determined on the basis of homo- and heteronuclear dipole-dipole couplings (residue indices for short range $|i-j|=2$, medium range $|i-j|=3$

or 4, long-range,|i-j|≥5). For ^{13}C-^{13}C distances, reduced ^{13}C-labelling patterns based on 1,3- and 2-^{13}C glycerol are essential because they facilitate the measurement of long-range couplings since dipolar truncation is avoided. In addition, C13, C20-$^{13}C_2$-retinal was incorporated to obtain retinal-protein contacts. In case of ASR, carbon-carbon restraints were determined based on 2D PDSD/DARR and proton-proton restraints by 2D CHHC spin diffusion experiments resulting in predominantly medium- and long-range restraints of up to 10 Å. These data sets were complemented by 3D homogeneously broadened rotational resonance (HBR2) NCOCX experiments to obtain additional restraints from the side chains. More long-range restraints were gained through the use of paramagnetic relaxation enhancement (PRE). This experiment requires site-specific protein labelling, often chemically via cysteines, with stable paramagnetic compounds such as for example nitroxides (MTSL). The dipolar interaction between the unpaired electron in these probes with ^{13}C and ^{15}N nuclei within the protein is long range (up to 15 -20 Å) and results in shortened T_1 and T_2 relaxation times. The latter represents itself in a distance-dependent line broadening and hence reduced peak intensity (r^{-6}) [58,59]. Such long-range constraints are extremely valuable for 3D structure determination in both solution- and solid-state NMR. They have been used here to refine the protomer structure and to define the oligomer interface and the oligomer arrangement (see subsection below) [60].

Structure calculation

The experimental data (chemical shifts/dihedral angles, distance restraints) need to be included into a structure calculation algorithm. In case of ASR, CNS 1.21 and ARIA 2.3 were used [61,62]. First, the structure of the ASR monomer was determined by excluding inter-protomer restraints (previously determined by PRE), which converged into a monomeric, heptahelical structure with a backbone r.m.s.d. of 0.8 Å [8]. A further refinement was carried out using inter-protomer PRE as well as EPR double electron-electron resonance (DEER) restraints, by which the native trimeric structure of ASR was mapped (see subsection below) [39]. Knowledge about the oligomeric order itself was available through a wealth of biochemical data.

Differences between the NMR and X-ray structures of ASR

The refined solid-state NMR structure shows in general good agreement with the X-ray structure [63] in terms of helical packing around the Schiff base. Conserved residues in the retinal-binding pocket as well as in the conserved cytoplasmic cluster of polar residues, responsible for the ASR photosensory function, are found in the NMR structure at positions very close to those in the crystal structure. There are however three key differences between both structures: (i) The NMR structure in agreement with other data is a lipid-stabilized homo-trimer with helices A, B and D', E' facing each other. In crystals, ASR forms undulating layers of dimers, stabilized by hydrophobic interactions between only helices D

of two monomers and with antiparallel oriented retinals. (ii) A beta-hairpin structure in the periplasmic BC loop present in the NMR structure, a conserved structural feature among microbial rhodopsins, seems disordered in the X-ray structure. Furthermore, the cytoplasmic sites of helices A and E are tilted away from the centre of the seven α-helical bundle in the NMR structure, but do not show this tilt in the crystal structure, which could be caused by the different oligomeric states and protein-protein contacts within the crystal. (iii) The NMR data show clearly 100% all-*trans* retinal whereas the crystal structure suggests a mixture between all-*trans* and 13-*cis*.

It is likely that for a detailed understanding of the protein beyond the retinal binding pocket, for example for phenomena involving the oligomeric interface, the knowledge of the correct protein orientation and interface as given by the solid-state NMR structure is crucial.

Probing the conformational dynamics of microbial rhodopsins by solid-state NMR

A resonance assignment is not only a starting point for a 3D structure determination but provides also the foundation for probing conformational dynamics of microbial rhodopsins within lipid bilayers.

A relatively straightforward approach is offered by H/D exchange experiments. Replacing an exchangeable amide proton by a deuteron will reduce the NMR intensities of the corresponding amide nitrogen in the protein backbone. The deduction in peak intensity depends on the H/D exchange rate, which is affected by the conformational dynamics of the protein. In this way, differences in conformational equilibria under dark and light conditions can be resolved as shown for ASR [64]. Another possibility is to use dipole-dipole couplings as dynamic reporters. The strong heteronuclear N-H or C-H dipole couplings of directly bonded nuclei will be scaled down in the presence of dynamics. This will affect ^{13}C and ^{15}N peak intensities as shown for SR II and proteorhodopsin [65,66] and enables to discriminate between rigid and mobile regions within the protein (e.g. helices or rigid loops vs. flexible loops). The exact measurement of these dipole couplings also enables to define site-resolved order parameters within the protein as shown for ASR and SR II [67,66].

Probing alterations in conformational dynamics is especially interesting in systems, which form functional complexes with subunits as for example in case of SR II. Its interaction with the transducer were monitored based on chemical shift perturbations and complemented by the analysis of peak intensities upon complex formation and light activation [66].

5. Oligomer Interactions

Membrane proteins often form homo-oligomers in lipid bilayers. The view on microbial rhodopsins was shaped for decades by the most-studied bacteriorhodopsin, which forms trimers packed in hexagonal, two-dimensional crystalline arrays [68]. With the discovery of many new microbial

rhodopsins at the beginning of the century, evidence started to appear that especially eubacterial rhodopsins form larger oligomeric complexes.

In an attempt to prepare 2D crystals of green proteorhodopsin [69], large 'donut' shaped structure could first be observed by cryo-EM, which were then resolved as hexamers by AFM [70]. Interestingly, the protein assembled into a pentameric state in non-crystalline membrane areas in these samples, which was then confirmed by native MS and blue native-PAGE analysis as the predominant form of green PR in DDM and after reconstitution into lipid bilayers [71,72]. A global picture emerged with a systematic study using a novel high-speed AFM method on a number of microbial rhodopsins which revealed that indeed eubacterial rhodopsins predominantly form pentamers while archaeal rhodopsins exist as trimers within the membrane [15]. However, no unified interaction pattern yielding to such complexes could be identified. These finding raise the question whether the observed homo-oligomeric assemblies are of functional relevance and whether the corresponding oligomer-interfaces could be analysed in terms of functionally and/or structurally relevant interactions. Such data can indeed be obtained by solid-state NMR as outlined below.

NMR on mixed-labelled oligomers

The possibility to prepare mixed-labelled complexes offers an attractive opportunity for visualizing cross-protomer contacts by NMR. The basic idea is illustrated in Fig. 5a for the green PR pentamer [71]: The oligomer can be assembled from differently labelled monomers (e.g. using U-^{13}C- and U-^{15}N-PR) resulting in a mixed-labelled pentamer. Interactions across the interface can now be measured by recording through-space ^{13}C-^{15}N dipolar correlation spectra to visualize cross-protomer side chain - side chain contacts. To achieve this goal, suitable conditions have to be found by which the oligomerisation can be controlled in a reversible fashion. This is very much protein-specific. For example, the monomeric state of *Gloeobacter* rhodopsin can be controlled by pH [73]. Another possible parameter is the choice of detergent [74]. PR forms mainly pentamers in dodecyl β-maltoside (DDM) and remains in that state after reconstitution into lipid bilayers [71]. However, solubilization e.g. in octyl glucoside (OG) or Triton X-100 TX-100 leads mainly to monomers. Therefore, solubilized ^{15}N-PR and ^{13}C-PR monomers could be mixed in a 1:1 ratio followed by reconstitution into lipid bilayers. In the bilayer, the protein assembles again into pentamers, which will then consist of ^{13}C and ^{15}N protomers as illustrated in Fig. 5a.

Monitoring these oligomeric states when searching for the optimal sample preparation procedure is of course essential. While numerous methods such es SEC or native MS are available for the detergent solubilized state, assessing the oligomer after reconstitution is more challenging. Suitable approaches would be for example cw and pulsed EPR (DEER) [75,76] or AFM [15]. However, these powerful and specialized methods would be too laborious for screening preparation conditions. One alternative is

offered by blue native-PAGE analysis, which has turned out to be a convenient way to assess the complex size before and after reconstitution. It is a non-denaturing procedure to analyse protein complexes in a native, folded state [77]. Coomassie Brilliant Blue G250 is used as the charge shift molecule, which retains the oligomeric state of protein complexes and which substitutes lipids in case of membrane proteins. Only a small amount of detergent is added to assist this process but does not solubilize or to disrupt the complex. The observed oligomeric state reflects the complex size within liposomes and agrees well with AFM data of PR in lipid bilayers [71,70].

The preparation of mixed-labelled proteorhodopsin complexes in this way results in 8 differently populated configurations in which the ^{13}C and ^{15}N protomers are arranged within the pentamer. Averaged over the whole ensemble, only 2.5 ^{15}N-^{13}C interfaces occur per pentamer and only 1.25 would have the correct side chain combination to contribute to ^{13}C-^{15}N cross-protomer cross peaks. Fortunately, the expected weak NMR signals from such a reduced number of interacting spins can be compensated by the use of sensitivity enhancement through DNP. Using dipolar through-space ^{15}N-^{13}C correlation experiments (TEDOR), dipolar interactions between coupled ^{13}C and ^{15}N nuclei within a range of 5 Å can be measured. If ^{15}N-containg side chains of residues such as e.g. Arg or Lys are within this distance range to ^{13}C-labelled side chains of Asp or Glu (Fig. 5a), characteristic cross peaks in 2D TEDOR spectra occur, which are a spectroscopic representation of a cross-protomer salt bridge. An example is shown in Fig. 5b. The ^{15}N-^{13}C TEDOR spectrum reveals an Arg-Asp cross peak for a mixed-labelled ^{13}C/^{15}N PR pentamer. This signal is not observed in uniformly labelled complexes and also disappears upon mutating R51 and D52, providing evidence for a cross-protomer salt bridge formed by these residues, which is important for the pentamer stabilization.

Based on this mixed-labelling approach and by varying the labelling schemes, a number of additional interactions can be identified. One further example is the cross-protomer contact between Trp34 and His75 in green PR (Fig. 5a) [14], which appears of direct functional relevance as outlined below.

Interface interactions during the photocycle

Testing the functional relevance of the homo-oligomers is not a trivial task as this would require performing comparative experiments on the native oligomer and on a monomer under identical conditions. However, the factors which affect the oligomerisation (e.g. detergent, pH, certain mutations) might also influence the functional mechanism and disentangling these effects from each other is difficult. A solution to this problem is to probe interactions at the protomer interfaces during the photocycle utilizing light-induced cryo-trapping as explained above. An example for green PR is shown in Figs. 5a and c: His75 interacts with W34 across the interface but also with the proton acceptor Asp97 within the same protomer [14,78], which has also been seen for blue PR by X-ray crystallography [79]. Mutation on all three residues have strong effects on the photocycle. Histidine is a highly

responsive residue often involved in enzymatic mechanisms because its imidazole side chain can adopt a positively charged and two neutral states (Nε2/τ, Nδ1/π). In solution, τ and π tautomers occur at a 4:1 ratio. His75 is highly conserved within the PR family, which raises the question about its state and role in these proteins. Histidines can be conveniently $^{13}C/^{15}N$ labelled in *E. coli* and a potential background from a His-tag can be prevented by removing it through a TEV cleavage site. The ^{13}C and ^{15}N chemical shifts of the histidine side chain atoms Nδ1, Nε2, Cγ and Cδ2 are sensitive markers for its charge and tautomeric state and reveal that His75 in the green PR dark state is primarily found as τ with only a small π-subpopulation. The corresponding DNP-enhanced ^{15}N spectrum is shown in Fig. 5c. Surprisingly, upon trapping the M-state, H75 is completely converted into the π-state and no τ-state signals are detected.

The observed tautomer conversion is also associated with an altered orientation of the imidazole side chain. ^{15}N-^{15}N PDSD through space correlation spectra reveal a clear cross peak between the His75(τ) amid nitrogen and Nδ1 but not with Nε2 in the M-state. However, this peak is not observed in the dark state (Fig. 5c) showing that His75 responds directly to the photocycle by altering its tautomeric state and conformation, which modulates its interactions with Trp34 and Asp97. Such a cross-protomer Asp-His-Trp triad could play a role in regulating photocycle and transport kinetics for example in response to an altered environmental pH. Interestingly, histidines are also found at protomer interfaces of other pentameric rhodopsins such as KR2 [80]. These approaches presented here are therefore of general relevance to understand related microbial rhodopsins.

In summary, solid-state NMR experiments showed for the first time functionally relevant cross-protomer interactions, which affect the photocycle. Especially interesting is the tautomeric and rotameric change of His75 at the interface during the photoreaction. These findings suggest further studies on other rhodopsins to elucidate if similar relationships exist.

The use of PREs for probing cross-protomer interfaces

The approach explained above relies on DNP-enhanced MAS NMR, which is great for cryo-trapping photointermediate states but comes at the cost of lower resolution and requires therefore especially tailored experiments resulting in higher spectral selectivity. An alternative approach is offered by the use of paramagnetic relaxation enhancement (PRE). If the probes are strategically well placed, PREs can be used not only in the context of refining 3D structures but also for analysing protomer interfaces as demonstrated for the trimeric ASR within lipid bilayers [60]. In this study, a cysteine mutation was introduced in helix A (S26C) and spin-labelled with MTSL (see Fig. 5d). As expected, residues in close proximity to the spin label (helices A and B) show the strongest reduction in intensity Fig. 5d). However, also strong effects are seen in helices D and E, which cannot be explained by intra-protomer PREs since they would be too far away from the MTSL spin label. Thus, they must arise from helices D and E at

the interface between adjacent protomers (Fig. 5d). Using these data, the interface can be mapped and 3D structure calculations can be improved. For unambiguous data interpretation, it is important to carry out dilution experiments with diamagnetic samples, to assess the spin-labelling efficiency and to validate that cys-mutations have no essential structural or functional consequences.

Site-directed spin labelling also offers the possibility to determine electron-electron distances between protomers by cw and pulsed, dipolar EPR spectroscopy (PELDOR/DEER), which has been extensively applied to microbial rhodopsins [75]. In contrast to PREs, only a single distance can be obtained per sample but these are very valuable because they are long-range (up to 70 Å) and relatively precise so that protomers arrangements can be resolved [81] and NMR structures can be refined [39].

6. Summary and perspective

Solid-state NMR based on MAS offers versatile experimental possibilities for rhodopsins and two branches of applications have emerged, which differ in terms of experimental design and conditions: Light-induced trapping of photointermediates benefits significantly from the sensitivity boost provided by DNP. The requirement for low temperatures for trapping as well as for DNP makes it a perfect match, but often requires well-tailored experimental schemes including selective isotope labelling to deal with the spectral complexity caused by freezing-induced heterogeneity. In contrast highly resolved spectra of uniformly labelled samples can be obtained on non-frozen samples of ground state rhodopsins allowing a global analysis of their structure and conformational dynamics. But what is the perspective of solid-state NMR in the context of other spectroscopic and structural methods? An important advantage is certainly the possibility to keep the rhodopsins within proteoliposome preparations and to maintain their native oligomeric state. Furthermore, 3D structures alone are not sufficient for deciphering the subtle molecular details leading to such a variety of functions and which control photocycle kinetics or colour adaptation. NMR can provide important additional site-resolve data e.g. on protonation states of side chains, on sub-Angstrom bond distortions within the chromophore, on the nature of hydrogen bonds or on the electronic environment of sites of interest. NMR parameters such as chemical shifts and dipole-dipole couplings are highly sensitive to these factors and are based on well-established theoretical foundations. NMR offers therefore an excellent link between structure and function. Hence, it would by desirable to connect 3D structures with functional, optical, vibrational and NMR data. Especially promising appears the link with QM/MM approaches [82,83,54,84]. Complex systems become increasingly accessible by methods such as automated fragmentation, which scales linearly with the number of atoms [85] and through which spectroscopic and structural data could be combined in a unified model in the future.

Figures and legends

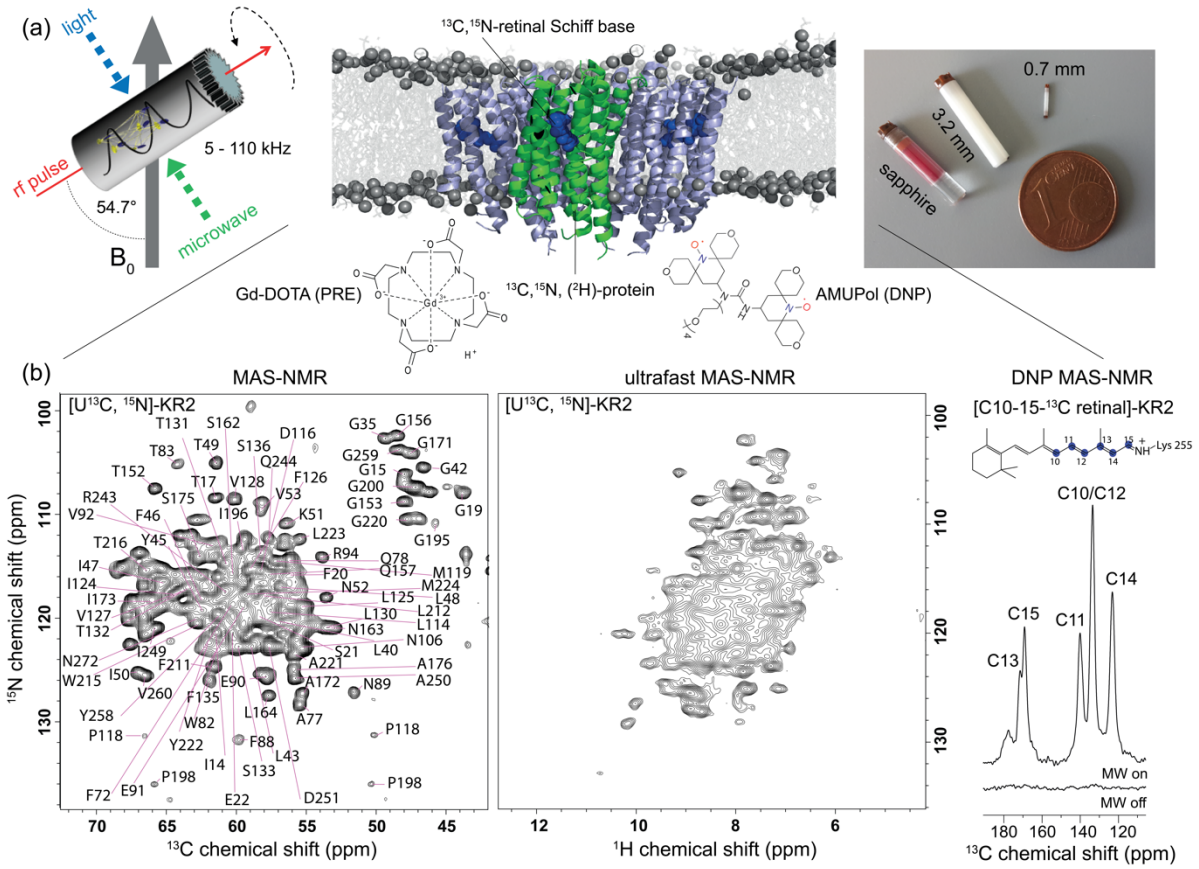

Fig. 1: Solid-state NMR on microbial rhodopsins. (a) MAS-NMR optionally coupled with *in situ* sample illumination for preparing photointermediates and microwave irradiation for DNP (left). Typically, 3.2 mm sapphire rotors are used for irradiation experiments (here filled with PR proteoliposomes). Ultrafast spinning requires even smaller rotors with just 0.7 mm diameter (right). Isotope labelled microbial rhodopsins such as pentameric PR or KR2 are embedded within lipid bilayers. Paramagnetic compounds can be added for PRE or DNP. **(b)** Example MAS-NMR spectra of the light-driven sodium pump KR2 in DMPC/DMPA lipid bilayers: ^{13}C detected NCA spectrum (left; 850 MHz, 14 kHz MAS, 12 mg KR2, pH 8.5, 280 K); ^{1}H-detected HN spectrum using ultra-fast MAS-NMR (middle; 850 MHz, 110 kHz MAS, 0.2 mg KR2, pH 6.0, 280 K); DNP-enhanced ^{13}C spectrum of C10-15-$^{13}C_6$-retinal within KR2 showing a 50-fold signal enhancement (right; 263 GHz/400 MHz, 8 kHz MAS, 10 mg KR2, AMUPol, 110 K) [16].

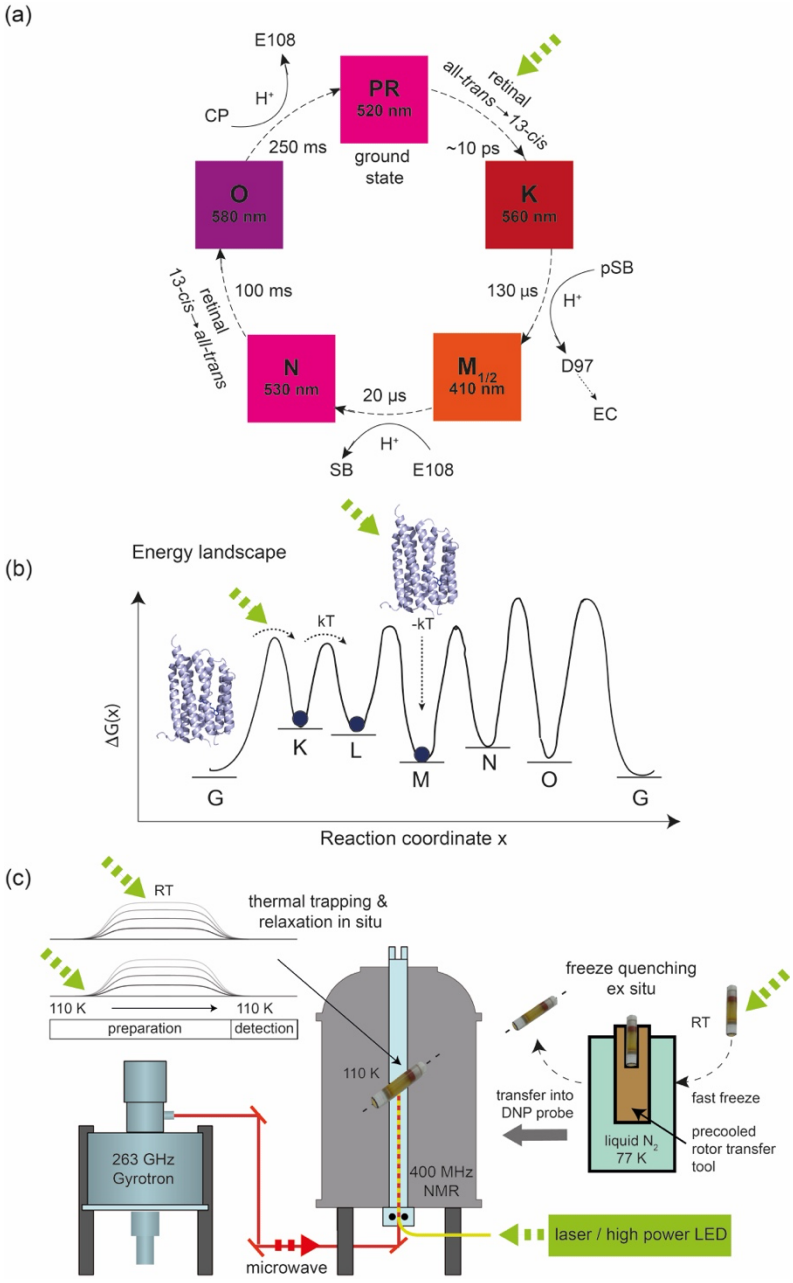

Fig. 2: Catching photointermediate states: (a) Schematic photocycle of green PR [42]. Photointermediates are characterized by their absorption maximum and their lifetime. **(b)** They can be trapped by a suitable choice of illumination and cooling conditions. For example, the K-state can be created by irradiating and measuring the sample at low temperature (110 K). Subsequent intermediates could be reached thermally or by illumination at higher temperatures followed by cooling. **(c)** Experimental setup for cryo-trapping of photointermediates for DNP-enhanced solid-state NMR. Using thin films of proteoliposomes within sapphire MAS rotors ensure sufficient light penetration. Lasers or high-power LEDs are suitable light sources. Illumination takes place within the spectrometer for thermal trapping/relaxation approaches or outside when utilizing freeze quenching. DNP enhanced MAS NMR spectra are usually recorded at low temperature (90-110 K).

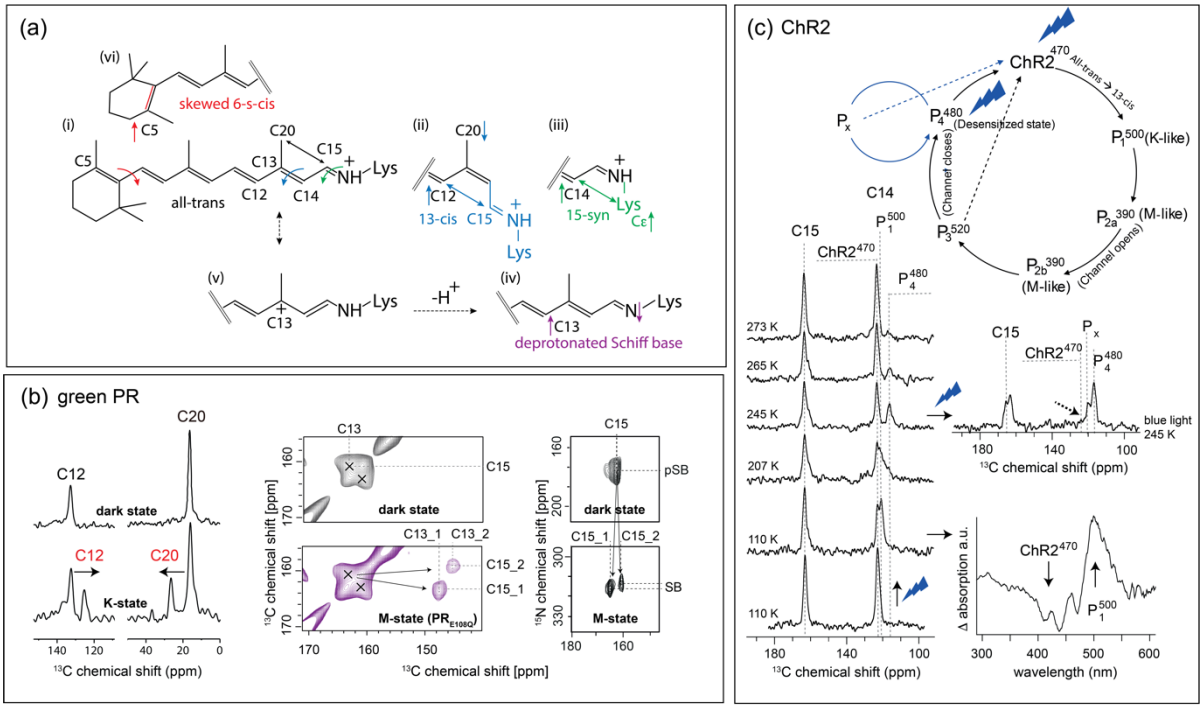

Fig. 3: NMR readouts for the conformation of the retinal Schiff base chromophore and example spectra. (a) Key NMR parameters for the conformation of the retinal Schiff base chromophore in rhodopsins. Increased shielding (↑), deshielding (↓), and relevant distances (↔) are indicated (see text for further details). These changes are in the range of 5 to 15 ppm for shielding/deshielding. Distances change by around 0.8 Å. **(b)** Trapping green PR photointermediates: K-state (left) [11], M-state (middle, right) [24]. **(c)** Trapping ChR2 photointermediates [30]: Schematic photocycle of ChR2 (top). The late desensitized state P_4^{480} shows a strong shielding of ^{13}C14 indicative of a 15-*syn* conformation. The cryo-UV-vis spectrum recorded after illumination at 150 K shows as an additional control ground state depopulation and K-like increase

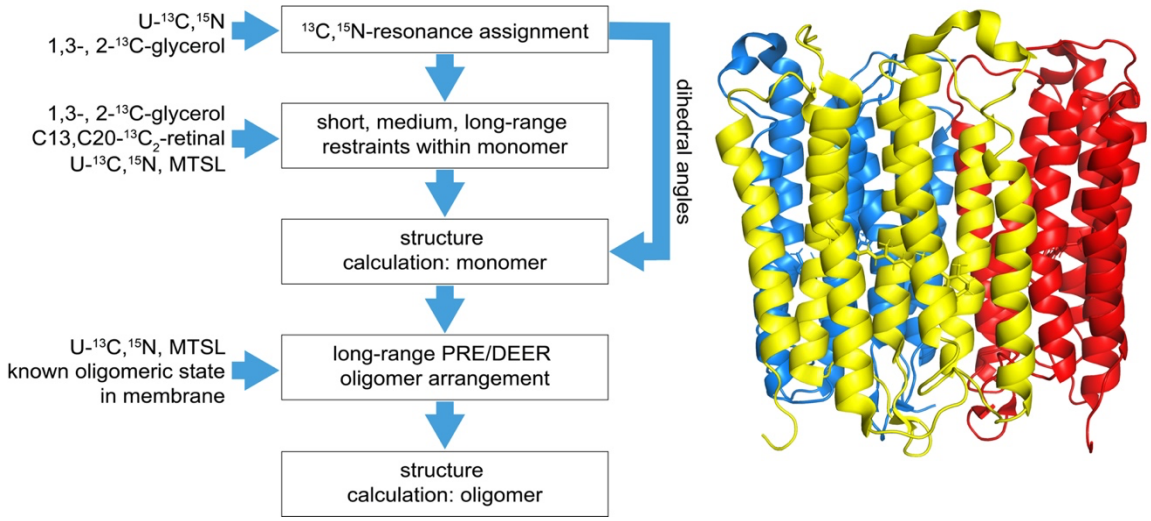

Fig. 4: Determination of the trimeric 3D structures of Anabaena Sensory Rhodopsin (ASR) within lipid bilayers by solid-state NMR [8]. The flow chart represents necessary samples and required experimental steps. The 3D structure shown here was refined by PRE and DEER long-range constraints (5UK6) [39].

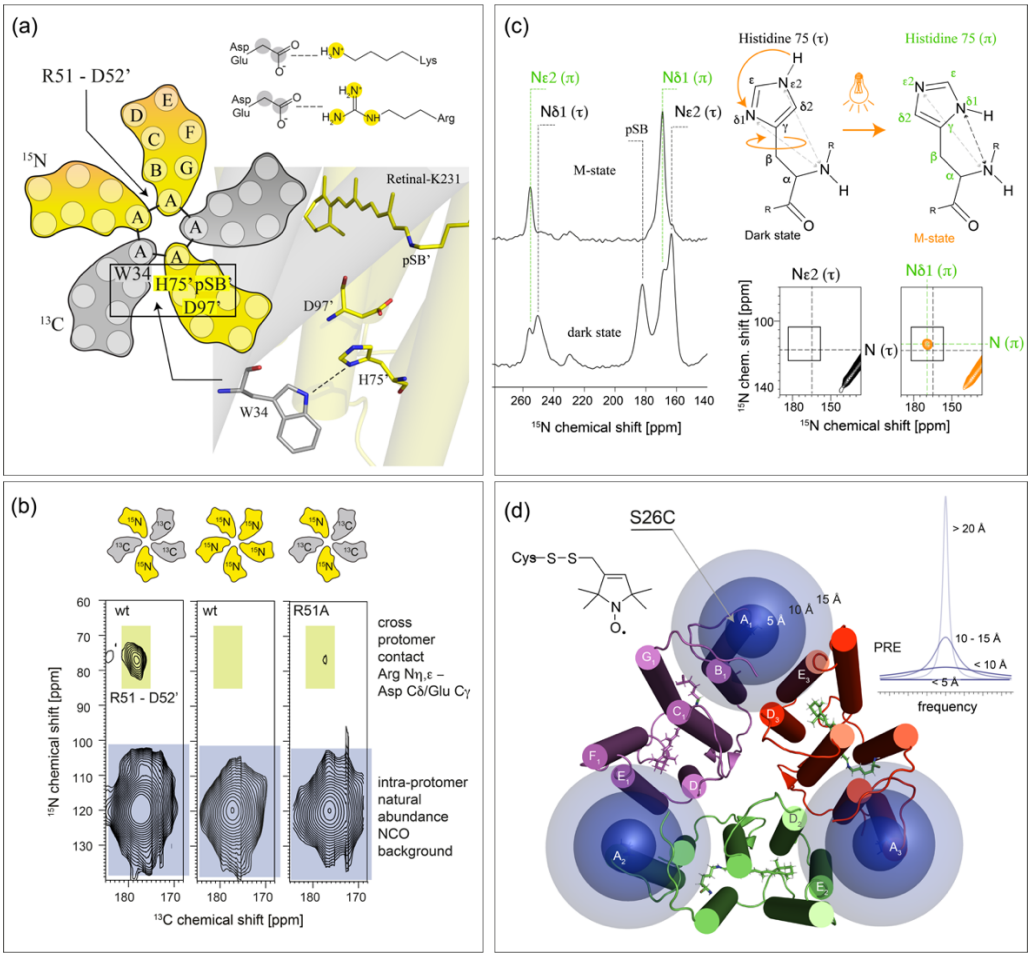

Fig. 5: Probing interactions at the oligomerisation interfaces of microbial rhodopsins by solid-state NMR. (a) Preparing mixed-labelled PR $^{13}C/^{15}N$ oligomers offers the possibility to identify interactions across the protomer interfaces such as Lys-Asp/Glu or Arg-Asp/Glu salt bridges. Specific interactions between Arg51-Asp52' and Trp34-His75' were found by DNP-enhanced solid-state NMR [14,71]. **(b)** Representative dipolar ^{15}N-^{13}C TEDOR spectrum of mixed-labelled green PR pentamers. The cross peak between $^{15}N\eta\varepsilon$-Arg51 and Cγ-Asp51' cannot be observed in uniformly ^{15}N-labelled complexes and also disappears upon mutating Arg51 or Asp52 [71]. The NCO cross peak arises from the correlation of ^{15}N and ^{13}C enriched sites with the natural abundance background of their neighbours (1.1.% ^{13}C, 0.4% ^{15}N). **(c)** Residue His75 at the protomer interface of green PR participates in the photocycle by switching its tautomer in the M-state from τ to π (spectra left). His75 also changes the imidazole ring orientation in the M-state as observed by through-space ^{15}N-^{15}N PDSD spectra. Only in the M-state, a cross peak between an imidazole and the backbone nitrogen can be observed. His75 seems to mediate an interaction between Trp34 and Asp97' across the interface [14]. **(d)** Probing cross-protomer interfaces by PREs as shown for trimeric ASR. Site-directed spin-labelling of Cys26 with MTSL enhances the nuclear spin relaxation properties depending on r^{-6}, which is observed by a reduced peak height. The spin label creates cross-protomer PREs in helices D and E [60]. The graphical representation is based on the PRE and EPR-refined solid-state NMR structure (PDB: 5UK6) [39].

References

1. Grote M, O'Malley MA (2011) Enlightening the life sciences: the history of halobacterial and microbial rhodopsin research. FEMS Microbiol Rev 35 (6):1082-1099. doi:10.1111/j.1574-6976.2011.00281.x

2. Govorunova EG, Sineshchekov OA, Li H, Spudich JL (2017) Microbial Rhodopsins: Diversity, Mechanisms, and Optogenetic Applications. Annu Rev Biochem 86:845-872. doi:10.1146/annurev-biochem-101910-144233

3. Beja O, Spudich EN, Spudich JL, Leclerc M, DeLong EF (2001) Proteorhodopsin phototrophy in the ocean. Nature 411 (6839):786-789. doi:10.1038/35081051

4. Beja O, Aravind L, Koonin EV, Suzuki MT, Hadd A, Nguyen LP, Jovanovich SB, Gates CM, Feldman RA, Spudich JL, Spudich EN, DeLong EF (2000) Bacterial rhodopsin: evidence for a new type of phototrophy in the sea. Science 289 (5486):1902-1906. doi:10.1126/science.289.5486.1902

5. Inoue K, Ono H, Abe-Yoshizumi R, Yoshizawa S, Ito H, Kogure K, Kandori H (2013) A light-driven sodium ion pump in marine bacteria. Nat Commun 4:1678. doi:10.1038/ncomms2689

6. Nagel G, Szellas T, Huhn W, Kateriya S, Adeishvili N, Berthold P, Ollig D, Hegemann P, Bamberg E (2003) Channelrhodopsin-2, a directly light-gated cation-selective membrane channel. Proc Natl Acad Sci U S A 100 (24):13940-13945. doi:10.1073/pnas.1936192100

7. Jung KH, Trivedi VD, Spudich JL (2003) Demonstration of a sensory rhodopsin in eubacteria. Mol Microbiol 47 (6):1513-1522. doi:10.1046/j.1365-2958.2003.03395.x

8. Wang S, Munro RA, Shi L, Kawamura I, Okitsu T, Wada A, Kim SY, Jung KH, Brown LS, Ladizhansky V (2013) Solid-state NMR spectroscopy structure determination of a lipid-embedded heptahelical membrane protein. Nat Methods 10 (10):1007-1012. doi:10.1038/nmeth.2635

9. Carravetta M, Zhao X, Johannessen OG, Lai WC, Verhoeven MA, Bovee-Geurts PH, Verdegem PJ, Kiihne S, Luthman H, de Groot HJ, deGrip WJ, Lugtenburg J, Levitt MH (2004) Protein-induced bonding perturbation of the rhodopsin chromophore detected by double-quantum solid-state NMR. J Am Chem Soc 126 (12):3948-3953. doi:10.1021/ja039390q

10. Lansing JC, Hohwy M, Jaroniec CP, Creemers AF, Lugtenburg J, Herzfeld J, Griffin RG (2002) Chromophore distortions in the bacteriorhodopsin photocycle: evolution of the H-C14-C15-H dihedral angle measured by solid-state NMR. Biochemistry 41 (2):431-438. doi:10.1021/bi011529r

11. Mao J, Aladin V, Jin X, Leeder AJ, Brown LJ, Brown RCD, He X, Corzilius B, Glaubitz C (2019) Exploring Protein Structures by DNP-Enhanced Methyl Solid-State NMR Spectroscopy. J Am Chem Soc 141 (50):19888-19901. doi:10.1021/jacs.9b11195

12. Ding X, Sun C, Cui H, Chen S, Gao Y, Yang Y, Wang J, He X, Iuga D, Tian F, Watts A, Zhao X (2018) Functional roles of tyrosine 185 during the bacteriorhodopsin photocycle as revealed by in situ spectroscopic studies. Biochim Biophys Acta Bioenerg 1859 (10):1006-1014. doi:10.1016/j.bbabio.2018.05.011

13. Ni QZ, Can TV, Daviso E, Belenky M, Griffin RG, Herzfeld J (2018) Primary Transfer Step in the Light-Driven Ion Pump Bacteriorhodopsin: An Irreversible U-Turn Revealed by Dynamic Nuclear

Polarization-Enhanced Magic Angle Spinning NMR. J Am Chem Soc 140 (11):4085-4091. doi:10.1021/jacs.8b00022

14. Maciejko J, Kaur J, Becker-Baldus J, Glaubitz C (2019) Photocycle-dependent conformational changes in the proteorhodopsin cross-protomer Asp-His-Trp triad revealed by DNP-enhanced MAS-NMR. Proc Natl Acad Sci U S A 116 (17):8342-8349. doi:10.1073/pnas.1817665116

15. Shibata M, Inoue K, Ikeda K, Konno M, Singh M, Kataoka C, Abe-Yoshizumi R, Kandori H, Uchihashi T (2018) Oligomeric states of microbial rhodopsins determined by high-speed atomic force microscopy and circular dichroic spectroscopy. Sci Rep 8 (1):8262. doi:10.1038/s41598-018-26606-y

16. Kaur J, Kriebel CN, Eberhardt P, Jakdetchai O, Leeder AJ, Weber I, Brown LJ, Brown RCD, Becker-Baldus J, Bamann C, Wachtveitl J, Glaubitz C (2019) Solid-state NMR analysis of the sodium pump Krokinobacter rhodopsin 2 and its H30A mutant. J Struct Biol 206 (1):55-65. doi:10.1016/j.jsb.2018.06.001

17. Shi L, Ahmed MA, Zhang W, Whited G, Brown LS, Ladizhansky V (2009) Three-dimensional solid-state NMR study of a seven-helical integral membrane proton pump--structural insights. J Mol Biol 386 (4):1078-1093. doi:10.1016/j.jmb.2009.01.011

18. Etzkorn M, Martell S, Andronesi OC, Seidel K, Engelhard M, Baldus M (2007) Secondary structure, dynamics, and topology of a seven-helix receptor in native membranes, studied by solid-state NMR spectroscopy. Angew Chem Int Ed Engl 46 (3):459-462. doi:10.1002/anie.200602139

19. Lalli D, Idso MN, Andreas LB, Hussain S, Baxter N, Han S, Chmelka BF, Pintacuda G (2017) Proton-Based Structural Analysis of a Heptahelical Transmembrane Protein in Lipid Bilayers. J Am Chem Soc 139 (37):13006-13012. doi:10.1021/jacs.7b05269

20. Linser R, Dasari M, Hiller M, Higman V, Fink U, Lopez del Amo JM, Markovic S, Handel L, Kessler B, Schmieder P, Oesterhelt D, Oschkinat H, Reif B (2011) Proton-detected solid-state NMR spectroscopy of fibrillar and membrane proteins. Angew Chem Int Ed Engl 50 (19):4508-4512. doi:10.1002/anie.201008244

21. Ni QZ, Daviso E, Can TV, Markhasin E, Jawla SK, Swager TM, Temkin RJ, Herzfeld J, Griffin RG (2013) High frequency dynamic nuclear polarization. Acc Chem Res 46 (9):1933-1941. doi:10.1021/ar300348n

22. Hall DA, Maus DC, Gerfen GJ, Inati SJ, Becerra LR, Dahlquist FW, Griffin RG (1997) Polarization-enhanced NMR spectroscopy of biomolecules in frozen solution. Science 276 (5314):930-932. doi:10.1126/science.276.5314.930

23. Sauvee C, Rosay M, Casano G, Aussenac F, Weber RT, Ouari O, Tordo P (2013) Highly efficient, water-soluble polarizing agents for dynamic nuclear polarization at high frequency. Angew Chem Int Ed Engl 52 (41):10858-10861. doi:10.1002/anie.201304657

24. Mehler M, Eckert CE, Leeder AJ, Kaur J, Fischer T, Kubatova N, Brown LJ, Brown RCD, Becker-Baldus J, Wachtveitl J, Glaubitz C (2017) Chromophore Distortions in Photointermediates of Proteorhodopsin Visualized by Dynamic Nuclear Polarization-Enhanced Solid-State NMR. J Am Chem Soc 139 (45):16143-16153. doi:10.1021/jacs.7b05061

25. Leeder AJ, Brown LJ, Becker-Baldus J, Mehler M, Glaubitz C, Brown RCD (2018) Synthesis of isotopically labeled all-trans retinals for DNP-enhanced solid-state NMR studies of retinylidene proteins. J Labelled Comp Radiopharm 61 (13):922-933. doi:10.1002/jlcr.3576

26. Creemers AF, Kiihne S, Bovee-Geurts PH, DeGrip WJ, Lugtenburg J, de Groot HJ (2002) (1)H and (13)C MAS NMR evidence for pronounced ligand-protein interactions involving the ionone ring of the retinylidene chromophore in rhodopsin. Proc Natl Acad Sci U S A 99 (14):9101-9106. doi:10.1073/pnas.112677599

27. Dawadi PB, Lugtenburg J (2010) Synthesis and use of stable isotope enriched retinals in the field of vitamin A. Molecules 15 (3):1825-1872. doi:10.3390/molecules15031825

28. Makino Y, Kawamura I, Okitsu T, Wada A, Kamo N, Sudo Y, Ueda K, Naito A (2018) Retinal Configuration of ppR Intermediates Revealed by Photoirradiation Solid-State NMR and DFT. Biophys J 115 (1):72-83. doi:10.1016/j.bpj.2018.05.030

29. Munro RA, de Vlugt J, Ward ME, Kim SY, Lee KA, Jung KH, Ladizhansky V, Brown LS (2019) Biosynthetic production of fully carbon-13 labeled retinal in E. coli for structural and functional studies of rhodopsins. J Biomol NMR 73 (1-2):49-58. doi:10.1007/s10858-019-00225-9

30. Becker-Baldus J, Bamann C, Saxena K, Gustmann H, Brown LJ, Brown RC, Reiter C, Bamberg E, Wachtveitl J, Schwalbe H, Glaubitz C (2015) Enlightening the photoactive site of channelrhodopsin-2 by DNP-enhanced solid-state NMR spectroscopy. Proc Natl Acad Sci U S A 112 (32):9896-9901. doi:10.1073/pnas.1507713112

31. Hatcher ME, Hu JG, Belenky M, Verdegem P, Lugtenburg J, Griffin RG, Herzfeld J (2002) Control of the pump cycle in bacteriorhodopsin: mechanisms elucidated by solid-state NMR of the D85N mutant. Biophys J 82 (2):1017-1029. doi:10.1016/S0006-3495(02)75461-1

32. Lacabanne D, Meier BH, Bockmann A (2018) Selective labeling and unlabeling strategies in protein solid-state NMR spectroscopy. J Biomol NMR 71 (3):141-150. doi:10.1007/s10858-017-0156-z

33. Mehler M, Eckert CE, Busche A, Kulhei J, Michaelis J, Becker-Baldus J, Wachtveitl J, Dotsch V, Glaubitz C (2015) Assembling a Correctly Folded and Functional Heptahelical Membrane Protein by Protein Trans-splicing. J Biol Chem 290 (46):27712-27722. doi:10.1074/jbc.M115.681205

34. Fan Y, Shi L, Ladizhansky V, Brown LS (2011) Uniform isotope labeling of a eukaryotic seven-transmembrane helical protein in yeast enables high-resolution solid-state NMR studies in the lipid environment. J Biomol NMR 49 (2):151-161. doi:10.1007/s10858-011-9473-9

35. Janke C, Scholz F, Becker-Baldus J, Glaubitz C, Wood PG, Bamberg E, Wachtveitl J, Bamann C (2013) Photocycle and vectorial proton transfer in a rhodopsin from the eukaryote Oxyrrhis marina. Biochemistry 52 (16):2750-2763. doi:10.1021/bi301412n

36. Ward ME, Wang S, Munro R, Ritz E, Hung I, Gor'kov PL, Jiang Y, Liang H, Brown LS, Ladizhansky V (2015) In situ structural studies of Anabaena sensory rhodopsin in the E. coli membrane. Biophys J 108 (7):1683-1696. doi:10.1016/j.bpj.2015.02.018

37. Ullrich SJ, Holper S, Glaubitz C (2014) Paramagnetic doping of a 7TM membrane protein in lipid bilayers by Gd(3)(+)-complexes for solid-state NMR spectroscopy. J Biomol NMR 58 (1):27-35. doi:10.1007/s10858-013-9800-4

38. Becker-Baldus J, Glaubitz C (2018) Cryo-trapped Intermediates of Retinal Proteins Studied by DNP-enhanced MAS NMR Spectroscopy. eMagRes 7 (4):79-91. doi:10.1002/9780470034590.emrstm1552

39. Milikisiyants S, Wang S, Munro RA, Donohue M, Ward ME, Bolton D, Brown LS, Smirnova TI, Ladizhansky V, Smirnov AI (2017) Oligomeric Structure of Anabaena Sensory Rhodopsin in a Lipid

Bilayer Environment by Combining Solid-State NMR and Long-range DEER Constraints. J Mol Biol 429 (12):1903-1920. doi:10.1016/j.jmb.2017.05.005

40. Voinov MA, Good DB, Ward ME, Milikisiyants S, Marek A, Caporini MA, Rosay M, Munro RA, Ljumovic M, Brown LS, Ladizhansky V, Smirnov AI (2015) Cysteine-Specific Labeling of Proteins with a Nitroxide Biradical for Dynamic Nuclear Polarization NMR. J Phys Chem B 119 (32):10180-10190. doi:10.1021/acs.jpcb.5b05230

41. Naito A, Makino Y, Shigeta A, Kawamura I (2019) Photoreaction pathways and photointermediates of retinal-binding photoreceptor proteins as revealed by in situ photoirradiation solid-state NMR spectroscopy. Biophys Rev 11 (2):167-181. doi:10.1007/s12551-019-00501-w

42. Friedrich T, Geibel S, Kalmbach R, Chizhov I, Ataka K, Heberle J, Engelhard M, Bamberg E (2002) Proteorhodopsin is a light-driven proton pump with variable vectoriality. J Mol Biol 321 (5):821-838. doi:10.1016/S0022-2836(02)00696-4

43. Harbison GS, Smith SO, Pardoen JA, Winkel C, Lugtenburg J, Herzfeld J, Mathies R, Griffin RG (1984) Dark-adapted bacteriorhodopsin contains 13-cis, 15-syn and all-trans, 15-anti retinal Schiff bases. Proc Natl Acad Sci U S A 81 (6):1706-1709. doi:10.1073/pnas.81.6.1706

44. Buhl E, Eberhardt P, Bamann C, Bamberg E, Braun M, Wachtveitl J (2018) Ultrafast Protein Response in Channelrhodopsin-2 Studied by Time-Resolved Infrared Spectroscopy. J Phys Chem Lett 9 (24):7180-7184. doi:10.1021/acs.jpclett.8b03382

45. Eckert CE, Kaur J, Glaubitz C, Wachtveitl J (2017) Ultrafast Photoinduced Deactivation Dynamics of Proteorhodopsin. J Phys Chem Lett 8 (2):512-517. doi:10.1021/acs.jpclett.6b02975

46. Jeon J, Thurber KR, Ghirlando R, Yau WM, Tycko R (2019) Application of millisecond time-resolved solid state NMR to the kinetics and mechanism of melittin self-assembly. Proc Natl Acad Sci U S A 116 (34):16717-16722. doi:10.1073/pnas.1908006116

47. Harbison GS, Mulder PPJ, Pardoen H, Lugtenburg J, Herzfeld J, Griffin RG (1985) High-resolution carbon-13 NMR of retinal derivatives in the solid state. J Am Chem Soc 107 (17):4809-4816. doi:10.1021/ja00303a001

48. Englert G (1975) A 13C-NMR. Study of cis-trans isomeric vitamins A, carotenoids and related compounds. Helv Chim Acta 58 (8):2367-2390. doi:10.1002/hlca.19750580817

49. Farrar MR, Lakshmi KV, Smith SO, Brown RS, Raap J, Lugtenburg J, Griffin RG, Herzfeld J (1993) Solid state NMR study of [epsilon-13C]Lys-bacteriorhodopsin: Schiff base photoisomerization. Biophys J 65 (1):310-315. doi:10.1016/S0006-3495(93)81065-8

50. Thompson LK, McDermott AE, Raap J, van der Wielen CM, Lugtenburg J, Herzfeld J, Griffin RG (1992) Rotational resonance NMR study of the active site structure in bacteriorhodopsin: conformation of the Schiff base linkage. Biochemistry 31 (34):7931-7938. doi:10.1021/bi00149a026

51. Harbison GS, Herzfeld J, Griffin RG (1983) Solid-state nitrogen-15 nuclear magnetic resonance study of the Schiff base in bacteriorhodopsin. Biochemistry 22 (1):1-4. doi:10.1021/bi00270a600

52. Mao J, Do NN, Scholz F, Reggie L, Mehler M, Lakatos A, Ong YS, Ullrich SJ, Brown LJ, Brown RC, Becker-Baldus J, Wachtveitl J, Glaubitz C (2014) Structural basis of the green-blue color switching in proteorhodopsin as determined by NMR spectroscopy. J Am Chem Soc 136 (50):17578-17590. doi:10.1021/ja5097946

53. Feng X, Verdegem PJE, Lee YK, Sandstrom D, Eden M, BoveeGeurts P, deGrip WJ, Lugtenburg J, deGroot HJM, Levitt MH (1997) Direct determination of a molecular torsional angle in the membrane protein rhodopsin by solid-state NMR. J Am Chem Soc 119 (29):6853-6857. doi:DOI 10.1021/ja970710d

54. Bondar AN, Elstner M, Suhai S, Smith JC, Fischer S (2004) Mechanism of primary proton transfer in bacteriorhodopsin. Structure 12 (7):1281-1288. doi:10.1016/j.str.2004.04.016

55. Hong M (1999) Determination of multiple ***φ***-torsion angles in proteins by selective and extensive (13)C labeling and two-dimensional solid-state NMR. J Magn Reson 139 (2):389-401. doi:10.1006/jmre.1999.1805

56. Wishart DS, Sykes BD, Richards FM (1992) The chemical shift index: a fast and simple method for the assignment of protein secondary structure through NMR spectroscopy. Biochemistry 31 (6):1647-1651. doi:10.1021/bi00121a010

57. Shen Y, Delaglio F, Cornilescu G, Bax A (2009) TALOS+: a hybrid method for predicting protein backbone torsion angles from NMR chemical shifts. J Biomol NMR 44 (4):213-223. doi:10.1007/s10858-009-9333-z

58. Otting G (2010) Protein NMR Using Paramagnetic Ions. In: Rees DC, Dill KA, Williamson JR (eds) Annual Review of Biophysics, Vol 39, vol 39. Annual Review of Biophysics. pp 387-405. doi:10.1146/annurev.biophys.093008.131321

59. Nadaud PS, Helmus JJ, Hofer N, Jaroniec CP (2007) Long-range structural restraints in spin-labeled proteins probed by solid-state nuclear magnetic resonance spectroscopy. J Am Chem Soc 129 (24):7502-7503. doi:10.1021/ja072349t

60. Wang S, Munro RA, Kim SY, Jung KH, Brown LS, Ladizhansky V (2012) Paramagnetic relaxation enhancement reveals oligomerization interface of a membrane protein. J Am Chem Soc 134 (41):16995-16998. doi:10.1021/ja308310z

61. Brunger AT, Adams PD, Clore GM, DeLano WL, Gros P, Grosse-Kunstleve RW, Jiang JS, Kuszewski J, Nilges M, Pannu NS, Read RJ, Rice LM, Simonson T, Warren GL (1998) Crystallography & NMR system: A new software suite for macromolecular structure determination. Acta Crystallogr D Biol Crystallogr 54 (Pt 5):905-921. doi:10.1107/s0907444998003254

62. Bardiaux B, Malliavin T, Nilges M (2012) ARIA for Solution and Solid-State NMR. In: Shekhtman A, Burz DS (eds) Protein Nmr Techniques, Third Edition, vol 831. Methods in Molecular Biology. pp 453-483. doi:10.1007/978-1-61779-480-3_23

63. Vogeley L, Sineshchekov OA, Trivedi VD, Sasaki J, Spudich JL, Luecke H (2004) Anabaena sensory rhodopsin: a photochromic color sensor at 2.0 A. Science 306 (5700):1390-1393. doi:10.1126/science.1103943

64. Wang S, Shi L, Kawamura I, Brown LS, Ladizhansky V (2011) Site-specific solid-state NMR detection of hydrogen-deuterium exchange reveals conformational changes in a 7-helical transmembrane protein. Biophys J 101 (3):L23-25. doi:10.1016/j.bpj.2011.06.035

65. Yang J, Aslimovska L, Glaubitz C (2011) Molecular dynamics of proteorhodopsin in lipid bilayers by solid-state NMR. J Am Chem Soc 133 (13):4874-4881. doi:10.1021/ja109766n

66. Etzkorn M, Seidel K, Li L, Martell S, Geyer M, Engelhard M, Baldus M (2010) Complex formation and light activation in membrane-embedded sensory rhodopsin II as seen by solid-state NMR spectroscopy. Structure 18 (3):293-300. doi:10.1016/j.str.2010.01.011

67. Good DB, Wang S, Ward ME, Struppe J, Brown LS, Lewandowski JR, Ladizhansky V (2014) Conformational dynamics of a seven transmembrane helical protein Anabaena Sensory Rhodopsin probed by solid-state NMR. J Am Chem Soc 136 (7):2833-2842. doi:10.1021/ja411633w

68. Henderson R, Unwin PN (1975) Three-dimensional model of purple membrane obtained by electron microscopy. Nature 257 (5521):28-32. doi:10.1038/257028a0

69. Shastri S, Vonck J, Pfleger N, Haase W, Kuehlbrandt W, Glaubitz C (2007) Proteorhodopsin: characterisation of 2D crystals by electron microscopy and solid state NMR. Biochimica et biophysica acta 1768 (12):3012-3019. doi:10.1016/j.bbamem.2007.10.001

70. Klyszejko AL, Shastri S, Mari SA, Grubmuller H, Muller DJ, Glaubitz C (2008) Folding and assembly of proteorhodopsin. J Mol Biol 376 (1):35-41. doi:10.1016/j.jmb.2007.11.030

71. Maciejko J, Mehler M, Kaur J, Lieblein T, Morgner N, Ouari O, Tordo P, Becker-Baldus J, Glaubitz C (2015) Visualizing Specific Cross-Protomer Interactions in the Homo-Oligomeric Membrane Protein Proteorhodopsin by Dynamic-Nuclear-Polarization-Enhanced Solid-State NMR. J Am Chem Soc 137 (28):9032-9043. doi:10.1021/jacs.5b03606

72. Hoffmann J, Aslimovska L, Bamann C, Glaubitz C, Bamberg E, Brutschy B (2010) Studying the stoichiometries of membrane proteins by mass spectrometry: microbial rhodopsins and a potassium ion channel. Phys Chem Chem Phys 12 (14):3480-3485. doi:10.1039/b924630d

73. Iizuka A, Kajimoto K, Fujisawa T, Tsukamoto T, Aizawa T, Kamo N, Jung KH, Unno M, Demura M, Kikukawa T (2019) Functional importance of the oligomer formation of the cyanobacterial H(+) pump Gloeobacter rhodopsin. Sci Rep 9 (1):10711. doi:10.1038/s41598-019-47178-5

74. Hussain S, Kinnebrew M, Schonenbach NS, Aye E, Han S (2015) Functional consequences of the oligomeric assembly of proteorhodopsin. J Mol Biol 427 (6 Pt B):1278-1290. doi:10.1016/j.jmb.2015.01.004

75. Klare JP, Steinhoff HJ (2009) Spin labeling EPR. Photosynth Res 102 (2-3):377-390. doi:10.1007/s11120-009-9490-7

76. Edwards DT, Huber T, Hussain S, Stone KM, Kinnebrew M, Kaminker I, Matalon E, Sherwin MS, Goldfarb D, Han S (2014) Determining the oligomeric structure of proteorhodopsin by Gd3+ -based pulsed dipolar spectroscopy of multiple distances. Structure 22 (11):1677-1686. doi:10.1016/j.str.2014.09.008

77. Wittig I, Braun HP, Schagger H (2006) Blue native PAGE. Nat Protoc 1 (1):418-428. doi:10.1038/nprot.2006.62

78. Hempelmann F, Holper S, Verhoefen MK, Woerner AC, Kohler T, Fiedler SA, Pfleger N, Wachtveitl J, Glaubitz C (2011) His75-Asp97 cluster in green proteorhodopsin. J Am Chem Soc 133 (12):4645-4654. doi:10.1021/ja111116a

79. Ran T, Ozorowski G, Gao Y, Sineshchekov OA, Wang W, Spudich JL, Luecke H (2013) Cross-protomer interaction with the photoactive site in oligomeric proteorhodopsin complexes. Acta Crystallogr D Biol Crystallogr 69 (Pt 10):1965-1980. doi:10.1107/S0907444913017575

80. Kovalev K, Astashkin R, Gushchin I, Orekhov P, Volkov D, Zinovev E, Marin E, Rulev M, Alekseev A, Royant A, Carpentier P, Vaganova S, Zabelskii D, Baeken C, Sergeev I, Balandin T, Bourenkov G, Carpena X, Boer R, Maliar N, Borshchevskiy V, Buldt G, Bamberg E, Gordeliy V (2020) Molecular mechanism of light-driven sodium pumping. Nat Commun 11 (1):2137. doi:10.1038/s41467-020-16032-y

81. Stone KM, Voska J, Kinnebrew M, Pavlova A, Junk MJ, Han S (2013) Structural insight into proteorhodopsin oligomers. Biophys J 104 (2):472-481. doi:10.1016/j.bpj.2012.11.3831

82. Gansmuller A, Concistre M, McLean N, Johannessen OG, Marin-Montesinos I, Bovee-Geurts PH, Verdegem P, Lugtenburg J, Brown RC, Degrip WJ, Levitt MH (2009) Towards an interpretation of 13C chemical shifts in bathorhodopsin, a functional intermediate of a G-protein coupled receptor. Biochimica et biophysica acta 1788 (6):1350-1357. doi:10.1016/j.bbamem.2009.02.018

83. Toker Y, Langeland J, Gruber E, Kjaer C, Nielsen SB, Andersen LH, Bonin VA, Schapiro I (2018) Counterion-controlled spectral tuning of the protonated Schiff-base retinal. Phys Rev A 98 (4):6. doi:ARTN 043428
10.1103/PhysRevA.98.043428

84. Hoffmann M, Wanko M, Strodel P, Konig PH, Frauenheim T, Schulten K, Thiel W, Tajkhorshid E, Elstner M (2006) Color tuning in rhodopsins: the mechanism for the spectral shift between bacteriorhodopsin and sensory rhodopsin II. J Am Chem Soc 128 (33):10808-10818. doi:10.1021/ja062082i

85. He X, Wang B, Merz KM, Jr. (2009) Protein NMR chemical shift calculations based on the automated fragmentation QM/MM approach. J Phys Chem B 113 (30):10380-10388. doi:10.1021/jp901992p